Journal of Magnetic Resonance **152,** 217–226 (2001)
doi:10.1006/jmre.2001.2405, available online at http://www.idealibrary.com on IDEAL®

PISEMA Powder Patterns and PISA Wheels

Jeffrey K. Denny,*[,1] Junfeng Wang,† T. A. Cross,‡ and J. R. Quine§

*Department of Mathematics, Mercer University, Macon, Georgia 31207; †Institute of Molecular Biophysics, Florida State University, Tallahassee, Florida 32306; ‡National High Magnetic Field Laboratory and Department of Chemistry, Florida State University, Tallahassee, Florida 32310; and §National High Magnetic Field Laboratory and Department of Mathematics, Florida State University, Tallahassee, Florida 32306-4510

Received January 23, 2001; revised June 15, 2001; published online August 24, 2001

Resonance patterns observed in 2D PISEMA (polarization inversion spin exchange at magic angle) spectra from a transmembrane α-helix have been demonstrated to yield structural details of the protein. This paper presents a mathematical discussion of the PISEMA powder spectrum as the image in the frequency plane of a quadratic function from the sphere of unit vectors. The simplicity of this function allows easy calculation of the powder spectrum. Based on this analysis of powder patterns, four degeneracies are discussed which arise in determining possible orientations associated with PISA spectra. This paper also gives parametric equations for PISA wheels, which are specific patterns observed in PISEMA spectra of oriented peptides. These wheels are useful both in assigning the resonances and in determining the orientation of the helix with respect to the magnetic field. The union of these PISA wheels gives the entire powder spectrum.

Key Words: **PISEMA; solid-state NMR; powder pattern; PISA wheel; membrane protein.**

1. INTRODUCTION

Resonance patterns observed in 2D solid-state NMR from transmembrane α–helices and β–sheets provide structural details of the molecule (*1–3*). The PISEMA (polarization inversion spin exchange at magic angle) experiment (*4*) correlates anisotropic dipolar and chemical shift interactions for labeled proteins. The patterns observed in PISEMA spectra for oriented, labeled proteins have been termed *Polar Index Slant Angle (PISA) wheels* (*1, 2*). These wheels are useful both in assigning resonances and in determining the general orientation of α-helices and β-sheets with respect to the magnetic field. Further, PISEMA spectra of powder samples provide information on the general orientation of molecules that undergo axial rotation, without orienting the sample (*5*). Together with the high resolution seen in PISEMA spectra, these capabilities make PISEMA experiments into powerful tools for obtaining structural information about membrane proteins, which are frequently difficult to study using X-ray crystallography or solution NMR.

To examine the nature of PISEMA spectra, a general discussion of paired dipolar and chemical shift interactions can be done in terms of several parameters, including the principal values of the two tensors and the polar angles α and β expressing the unique principal axis of the dipolar tensor in the principal axis frame of the chemical shift tensor. Powder spectra for such paired interactions have been discussed previously by Linder *et al.* (*6*), and the general outlines of the spectrum were termed *ridge plots*. Most recently, Bak *et al.* developed a program, called SIMPSON, for simulating solid-state NMR spectroscopy which can calculate PISEMA powder spectra directly from the Hamiltonian (*7*). Other recent discussions of PISEMA powder spectra include (*5, 8–11*).

In light of the usefulness of PISEMA powder patterns and PISA wheels for obtaining structural information about transmembrane peptides, this paper is a mathematical discussion of computed PISEMA spectra. First, powder spectra are given as the image in the frequency plane of a function from the unit sphere. The simplicity of this function allows calculation of the ridge plots of PISEMA powder patterns without using Hamiltonians giving results very close to those found in (*6, 7*). Then, a complete analysis of the degeneracies in PISEMA data is presented, including straightforward formulas for determining peptide plane orientations from PISEMA resonances and a method for obtaining the sign of the dipolar interaction for PISEMA resonances in certain regions of spectra. These computations can then be applied to data for the M2 transmembrane peptide from influenza A and for gramicidin A. Finally, the mathematics of creating PISA wheels are discussed and applied to a two-parameter model of an ideal helix to produce parametric equations for PISA wheels and the resonance patterns on the wheels. Using this approach as a model of the M2 transmembrane peptide, we give an example of a mathematical method for fitting an ideal PISA wheel to actual data.

2. THEORY

A PISEMA experiment measures two tensors evaluated at a unit direction $\vec{B}_0$ for the magnetic field. This can be considered experimental determination of the value of a function from the unit sphere to the frequency plane. Here the case of a chemical shift tensor σ and a dipolar splitting tensor ν is considered, and the value of the function in the frequency plane is denoted

[1] To whom correspondence should be addressed. E-mail: denny_jk@mercer.edu.

1090-7807/01 $35.00

$\pi(\vec{B}_0) = (\sigma, \nu)$, where $\vec{B}_0$ is a vector with $|\vec{B}_0| = 1$. This function will be called the *PISEMA function.*

The chemical shift tensor σ is an asymmetric tensor. Its principal axis frame is denoted

$$\mathbf{PAF} = (\vec{\sigma}_{11},\ \vec{\sigma}_{22},\ \vec{\sigma}_{33}),$$

and the corresponding principal values are denoted σ_{11}, σ_{22}, and σ_{33}, with $\sigma_{11} \le \sigma_{22} \le \sigma_{33}$. The value of σ is given by

$$\sigma = \sigma_{11}(\vec{B}_0 \cdot \vec{\sigma}_{11})^2 + \sigma_{22}(\vec{B}_0 \cdot \vec{\sigma}_{22})^2 + \sigma_{33}(\vec{B}_0 \cdot \vec{\sigma}_{33})^2.$$

The dipolar tensor ν is traceless and axially symmetric with unique rotation axis $\vec{u}$ in the direction of a covalent bond. If $\nu_\parallel$ is the value of ν when $\vec{B}_0 = \vec{u}$, then

$$\nu = \frac{\nu_\parallel}{2}(3(\vec{B}_0 \cdot \vec{u})^2 - 1).$$

Because of the doublet splitting of the dipolar interaction, only the absolute value of ν can be experimentally determined. In the Results and Discussion section, methods of obtaining the sign of ν from PISEMA spectra for resonances in particular regions of some spectra will be described.

The polar angles giving the rotation axis of the dipolar tensor in the principal axis frame of the chemical shift tensor are denoted α and β, as in (*6*). Thus, α and β describe the relative orientation of the two tensors (see Fig. 1), and

$$\vec{u} = \cos\alpha \sin\beta \vec{\sigma}_{11} + \sin\alpha \sin\beta \vec{\sigma}_{22} + \cos\beta \vec{\sigma}_{33}.$$

To write equations for the PISEMA function π, let (x, y, z) be the coordinates of $\vec{B}_0$ in **PAF**. Then

$$\begin{aligned} \sigma &= \sigma_{11} x^2 + \sigma_{22} y^2 + \sigma_{33} z^2 \\ \nu &= \frac{\nu_\parallel}{2}(3(\cos\alpha \sin\beta\, x + \sin\alpha \sin\beta\, y + \cos\beta\, z)^2 - 1), \end{aligned} \qquad [1]$$

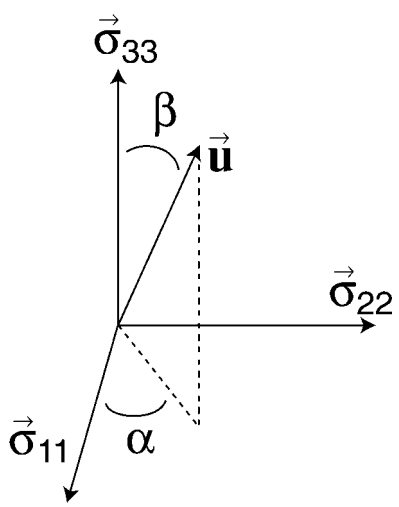

FIG. 1. The polar angles, α and β, give the orientation of the rotation axis, $\vec{u}$, of the dipolar tensor in the principal axis frame of the chemical shift tensor.

with $x^2 + y^2 + z^2 = 1$. Given in **PAF** coordinates (x, y, z), the function $\pi(\vec{B}_0) = (\sigma, \nu)$ will be denoted $\pi(x, y, z)$. These equations show that σ and ν are invariant under the inversion sending (x, y, z) to $(-x, -y, -z)$.

When $\alpha = 0^\circ$, the equations in [1] become

$$\begin{aligned} \sigma &= \sigma_{11} x^2 + \sigma_{22} y^2 + \sigma_{33} z^2 \\ \nu &= \frac{\nu_\parallel}{2}(3(\sin\beta x + \cos\beta z)^2 - 1). \end{aligned} \qquad [2]$$

These equations demonstrate that if $\alpha = 0$, then σ and ν are invariant under the reflection sending (x, y, z) to $(x, -y, z)$ as well as the rotation sending (x, y, z) to $(-x, y, -z)$; thus,

$$\pi(x, y, z) = \pi(x, -y, z) = \pi(-x, y, -z) = \pi(-x, -y, -z). \qquad [3]$$

3. MATERIALS AND METHODS

The calculations for this paper were performed on a Macintosh computer with a 333 MHz G3 processor and on a Gateway computer with a 350 MHz Celeron processor. The computation program *Maple 6* (Waterloo Maple, Inc.) was used for numeric and symbolic computations.

PISEMA data for oriented samples of the M2 transmembrane peptide of influenza A are used in computations in the following sections. From Song *et al.* (*12*), the chemical shift (±3 ppm) and dipolar splittings (±1 kHz) written as ordered pairs (σ, ν) at several sites are: Val^{27} (135 ppm, 6.85 kHz), Val^{28} (106 ppm, 2.0 kHz), Ile^{32} (129 ppm, 2.2 kHz), Ile^{33} (168 pmm, 3.75 kHz), Ile^{35} (118 ppm, 5.3 kHz), Ile^{39} (124 ppm, 4.4 kHz), and Ile^{42} (127 ppm, 6.6 kHz). The average values of the chemical shift tensor elements for these sites are used in computations in the following sections. Based on data from Song *et al.* (*12*), these average values are $\sigma_{11} = 31$, $\sigma_{22} = 55$, and $\sigma_{33} = 202$ ppm. The ^{15}N–^{1}H dipolar coupling constant is taken to be $\nu_\parallel = 10.735$ kHz. Finally, the polar angles of the rotation axis of the dipolar tensor in the principal axis frame of the chemical shift tensor are taken to be $\alpha = 0^\circ$ and $\beta = 17^\circ$, as in (*2, 12*).

PISEMA powder pattern data from Mai *et al.* (*13*) for gramicidin A are also used in calculations below. For these data, $\sigma_{11} = -60$, $\sigma_{22} = -37$, and $\sigma_{33} = 98$ ppm relative to $\sigma_{iso} = 0$ ppm. Also, the polar angles of the rotation axis of the dipolar tensor in the principal axis frame of the chemical shift tensor are again $\alpha = 0^\circ$ and $\beta = 17^\circ$. As in (*5*), the ^{15}N–^{1}H dipolar coupling constant is taken to be $\nu_\parallel = 11.335$ kHz.

4. RESULTS AND DISCUSSION

4.1. Orientations and Powder Spectra

If the coordinates (x, y, z) of $\vec{B}_0$ are known in **PAF**, then the *orientation* of **PAF** with respect to the magnetic field direction

is known; i.e., the **PAF** is known in the laboratory frame up to a rotation about $\vec{B}_0$. As in (*14*), this orientation is reported using the Euler angles ϕ and θ of the **PAF** in the laboratory frame so that $(x, y, z) = (\cos\phi \sin\theta, \sin\phi \sin\theta, \cos\theta)$. A PISEMA powder pattern is the image under the PISEMA function of all possible orientations of **PAF** in the laboratory frame. Mathematically, this is equivalent to saying that a PISEMA powder pattern is the image under the PISEMA function of all possible orientations of $\vec{B}_0$ in the **PAF**. Thus, given a PISEMA resonance (σ, ν), the number of orientations of $\vec{B}_0$ in **PAF** with $\pi(\vec{B}_0) = (\sigma, \nu)$ is the number of orientations of **PAF** consistent with a solid-state NMR anisotropic observation of (σ, ν) for the given resonance.

Considering just one transition of the doublet in the dipolar interaction, the ridge plot of the powder spectrum of a PISEMA experiment is boundary of the set of points $\pi(\vec{B}_0) = (\sigma, \nu)$ for all $\vec{B}_0$ on the unit sphere, i.e., the set of all points satisfying Eq. [1] for some (x, y, z) on the sphere. This ridge plot will be called the *singlet powder pattern*. If the doublet is taken into account, the powder pattern is the singlet together with its reflection in the line $\nu = 0$.

The intensity of the singlet pattern at a given resonance (σ, ν) is related to the number of orientations for which the PISEMA function π produces (σ, ν). Equation [1] shows that this number is at most 8, since three quadratic equations, in general, have at most 8 solutions. If $\alpha = 0^\circ$, Eq. [3] shows that there are at least 4 solutions if (σ, ν) is in the powder pattern. Since this number of orientations is greater than one, there are certain *degeneracies*, or *ambiguities*, that arise in finding orientations from PISEMA data. Understanding both the nature of these degeneracies and the process of how to eliminate them are important steps in obtaining orientational information from PISEMA data; this problem will be addressed in the next section.

Having discussed orientations, shapes of powder patterns are now considered. The powder pattern corresponding to $\alpha = 0^\circ$ and $\beta = 0^\circ$ is easiest to examine. Here the orientation of the **PAF** with $\vec{\sigma}_{11}$ in the direction of $\vec{B}_0$ is mapped by the PISEMA function to the point $R = (\sigma_{11}, -\nu_\parallel/2)$ in the frequency plane. Similarly, the orientation with $\vec{\sigma}_{22}$ in the direction of $\vec{B}_0$ is mapped to $Q = (\sigma_{22}, -\nu_\parallel/2)$, and the orientation with $\vec{\sigma}_{33}$ in the direction of $\vec{B}_0$ is mapped to $P = (\sigma_{33}, -\nu_\parallel/2)$. From Eq. [2] it is easy to see that the circle $x = 0$ on the sphere maps onto the line joining the points P and Q; the circle $y = 0$ maps onto the line joining P and R; and the circle $z = 0$ maps onto the line joining Q and R. The PISEMA function π maps the octant $x > 0$, $y > 0$, $z > 0$ of the sphere one-to-one onto the interior of the triangle formed by the points P, Q, and R (see Fig. 2). Every point of the interior of this triangle is covered 8 times by π, because all 8 of the points $(\pm x, \pm y, \pm z)$ are mapped onto the same point (σ, ν).

Next, consider the case $\alpha = 0$ and $0 < \beta < 90^\circ$. In this case, the circle $y = 0$ on the sphere maps to an ellipse rather than a line. Unit vectors of interest on this circle are $\vec{\sigma}_{33}$, $\vec{\sigma}_{22}$, $\vec{\sigma}_{11}$, $\vec{u}^\perp = \vec{\sigma}_{22} \times \vec{u}$, and $\vec{u}$; the PISEMA function maps these vectors

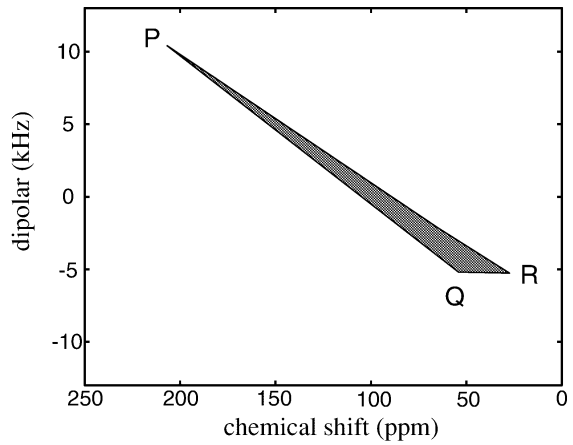

FIG. 2. A singlet powder pattern with $\alpha = 0^\circ, \beta = 0^\circ, \sigma_{11} = 35$ ppm, $\sigma_{22} = 55$ ppm, and $\sigma_{33} = 210$ ppm. Using the PISEMA function π, the orientation of **PAF** with $\vec{\sigma}_{11}$ in the direction of $\vec{B}_0$ is mapped to the point R. The orientation with $\vec{\sigma}_{22}$ in the direction of $\vec{B}_0$ is mapped to Q, and the orientation with $\vec{\sigma}_{33}$ in the direction of $\vec{B}_0$ is mapped to P. Note that the PISEMA function covers each point in the interior of the triangle 8 times.

to the points

$$
\begin{aligned}
P &= (\sigma_{33}, \nu_\parallel(3\cos^2\beta - 1)/2),\\
Q &= (\sigma_{22}, -\nu_\parallel/2),\\
R &= (\sigma_{11}, \nu_\parallel(3\sin^2\beta - 1)/2),\\
S &= (\sigma_{33}\sin^2\beta + \sigma_{11}\cos^2\beta, -\nu_\parallel/2), \text{ and}\\
T &= (\sigma_{33}\cos^2\beta + \sigma_{11}\sin^2\beta,\ \nu_\parallel),
\end{aligned}
$$

respectively (see Fig. 3).

To verify that the powder pattern shape in this case is an ellipse, substitute $y = 0$ in Eq. [2] and eliminate the variables x and z. The result is an implicit equation for the ellipse in the frequency plane with no units present, which can be plotted using the *Maple* command `implicitplot`. The ellipse equation is

$$(\tilde{\nu} - \cos 2\beta\,\tilde{\sigma} - \sin^2\beta)^2 = \tilde{\sigma}(1 - \tilde{\sigma})\sin 2\beta \qquad [4]$$

where

$$
\begin{aligned}
\tilde{\sigma} &= \frac{\sigma - \sigma_{11}}{\sigma_{33} - \sigma_{11}}\\
\tilde{\nu} &= \frac{1}{3}\left(\frac{2\nu}{\nu_\parallel} + 1\right).
\end{aligned}
\qquad [5]
$$

To complete the description of this powder pattern, note that great circles on the sphere containing $\vec{\sigma}_{22}$ and $-\vec{\sigma}_{22}$ go to lines that extend from the point $(\sigma_{22}, -\nu_\parallel/2)$ to points on the ellipse. The singlet powder pattern for this case is shown in Fig. 3.

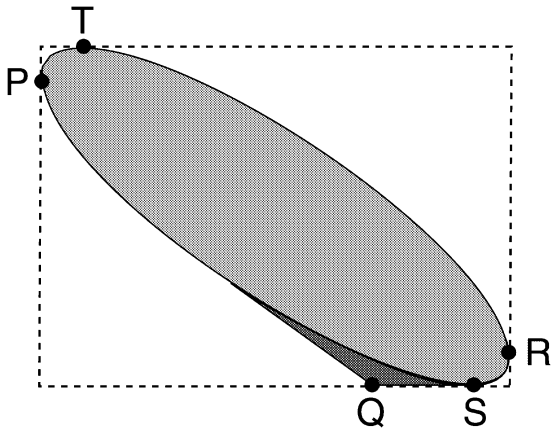

FIG. 3. A singlet powder pattern with $\alpha = 0^\circ$ and $\beta = 17^\circ$. The left and right boundary lines are $\sigma = \sigma_{33}$ and $\sigma = \sigma_{11}$, respectively, and the top and bottom lines are $\nu = \nu_\parallel$ and $\nu = -\frac{\nu_\parallel}{2}$, respectively. The orientations of the **PAF** with $\vec{\sigma}_{33}$, $\vec{\sigma}_{22}$, $\vec{\sigma}_{11}$, $\vec{u}^\perp = \vec{\sigma}_{22} \times \vec{u}$, and $\vec{u}$ parallel to $\vec{B}_0$ map to the points P, Q, R, S, and T, respectively. The PISEMA function π maps 4 points on the unit sphere onto each point in the light gray region and 8 points on the unit sphere to each point in the dark gray region.

Finally, consider the $\alpha \neq 0$ case. The general equation for ν in Eq. [1] depends on the square of the dot product

$$\vec{u} \cdot \vec{B}_0 = (\cos\alpha x + \sin\alpha y)\sin\beta + \cos\beta z. \qquad [6]$$

When $|\sin\beta|$ is relatively small, the influence of the angle α on the value of the dipolar splitting ν is severely limited. Thus, for small $|\sin\beta|$, PISEMA powder patterns with $\alpha = \pm 15^\circ$ are all essentially the same shape as seen above for $\alpha = 0$. When $|\sin\beta|$ is large, the powder pattern shape is greatly influenced by the value of α, and a wide array of shapes arise as shown in (*6, 11*). Such powder patterns can be produced using the PISEMA function π by plotting the images under π of a large number of great circles on the sphere.

In membrane proteins, small values of $|\sin\beta|$ are encountered in practice. For the M2 transmembrane peptide and for gramicidin A, the angle β has been determined (*13*) to be 17°, which has been shown to be typical for ^{15}N chemical shift tensors in nonglycine amides (*15–17*). The simulated ellipses for the doublet powder pattern for gramicidin A are shown in Fig. 4 and are similar to the powder pattern found in (*5*). Using Eq. [4], the foci of the ellipses can be found and used to compute the slopes of the major axes. These values are found to be ± 0.254 kHz/ppm, which compare favorably to the experimentally determined slopes of ± 0.270 kHz/ppm reported in (*5*).

The influence of the angle α is also very limited in residues whose the unique axis, $\vec{u}$, of the dipolar interaction is approximately parallel to $\pm\vec{B}_0$. In this case, $|z|$ is close to 1 and $|x|$, $|y|$ are close to 0 in Eq. [6]; hence, the value of α has little effect on PISEMA spectra of such residues. This situation arises in oriented samples of membrane proteins which have a small tilt with respect to the magnetic field direction, e.g., the membrane peptide AChR M2 (18).

4.2. Degeneracies

The PISEMA function π maps orientations on the sphere to the frequency plane. To obtain orientation information about a peptide plane from a PISEMA spectrum, the PISEMA function must be inverted (i.e., find the orientation of $\vec{B}_0$ that produced a particular resonance in the PISEMA spectrum). This involves solving the equations in [1] for (x, y, z), with $x^2 + y^2 + z^2 = 1$. It has been shown in the above sections, using the powder spectrum, that this system of equations has several solutions giving rise to degeneracies, or ambiguities, in the orientation of the principal axis frame. A further complication is that $|\nu|$ is the observable, and the sign of ν is not known. Thus, orientation information about peptide planes can only be determined if the degeneracies are resolved. The calculations below are done for the $\alpha = 0^\circ$ case and then the $\alpha \neq 0$ case. Subsequently, the $\alpha = 0^\circ$ case is applied to data for the M2 transmembrane peptide from influenza A.

For the $\alpha = 0^\circ$ case, suppose that a resonance in a PISEMA spectrum has chemical shift σ and dipolar splitting $|\nu|$. To describe the multiple solutions to the equations in [2] for (x, y, z) with $x^2+y^2+z^2 = 1$, a sequence of ± 1 values, ε_j, $j = 1, 2, 3, 4$ is defined. The first, ε_1, describes the sign degeneracy of ν,

$$\nu = \varepsilon_1|\nu|. \qquad [7]$$

With this notation, finding the orientation of the chemical shift principal axis frame with respect to $\vec{B}_0$ requires solving the system

$$\begin{cases} 1 = x^2 + y^2 + z^2 \\ \varepsilon_1|\nu| = \dfrac{\nu_\parallel}{2}(3(\sin\beta\, x + \cos\beta\, z)^2 - 1) \\ \sigma = \sigma_{11}\, x^2 + \sigma_{22}\, y^2 + \sigma_{33}\, z^2 \end{cases} \qquad [8]$$

for x, y, and z.

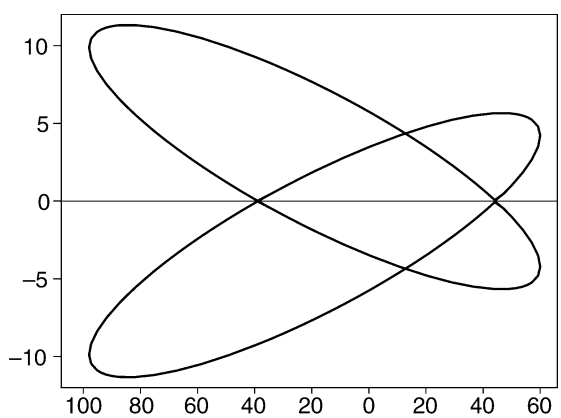

FIG. 4. A simulated doublet PISEMA powder pattern based on data for gramicidin A. The slope of the major axes of the ellipses are computed to be ± 0.254 kHz/ppm. The shape of the powder pattern and the slope of the major axes of the ellipses compare favorably with the experimental spectrum found in (*5*).

The value of ε_2 describes the sign degeneracy in solving the second equation in Eq. [8],

$$\sin\beta\, x + \cos\beta\, z = \varepsilon_2\sqrt{\frac{1}{3}\left(\frac{2\varepsilon_1|\nu|}{\nu_\parallel}+1\right)}. \qquad [9]$$

To produce a system equivalent to Eq. [8], solve the above equation for z and substitute into the third equation in Eq. [8]. Next, solve the first equation in Eq. [8] for z^2 and substitute into the third equation. This creates the equivalent system of equations

$$\begin{cases} 1 = x^2 + y^2 + z^2 \\ \sigma = (\sigma_{11}-\sigma_{33})\,x^2 + (\sigma_{22}-\sigma_{33})\,y^2 + \sigma_{33} \\ \sigma = (\sigma_{11}+\sigma_{33}\tan^2\beta)\,x^2 + \sigma_{22}\,y^2 \\ \qquad -\, 2\varepsilon_2\sigma_{33}\,\hat{\nu}\,x + \sigma_{33}\cot^2\beta\,\hat{\nu}^2, \end{cases} \qquad [10]$$

where

$$\hat{\nu} = \tan\beta\sec\beta\sqrt{\frac{1}{3}\left(\frac{2\varepsilon_1|\nu|}{\nu_\parallel}+1\right)}.$$

To find x, solve the second equation in Eq. [10] for y^2 and substitute into the third equation. This gives a quadratic equation of the form

$$Ax^2 - 2\varepsilon_2 Bx + C = 0,$$

where

$$A = \sigma_{11} + \sigma_{33}\tan^2\beta + \frac{\sigma_{22}(\sigma_{33}-\sigma_{11})}{\sigma_{22}-\sigma_{33}},$$

$$B = \sigma_{33}\tan\beta\sec\beta\sqrt{\frac{1}{3}\left(\frac{2\varepsilon_1|\nu|}{\nu_\parallel}+1\right)},$$

$$C = \frac{\sigma_{33}\sec^2\beta}{3}\left(\frac{2\varepsilon_1|\nu|}{\nu_\parallel}+1\right) - \sigma + \frac{\sigma_{22}(\sigma-\sigma_{33})}{\sigma_{22}-\sigma_{33}}.$$

This equation can be solved using the quadratic formula

$$x = \frac{\varepsilon_2 B + \varepsilon_3\sqrt{B^2-AC}}{A}, \qquad [11]$$

and this defines ε_3. The final degeneracy, ε_4 is then encountered when solving for y,

$$y = \varepsilon_4\sqrt{1-x^2-z^2}. \qquad [12]$$

Thus, if the values of ε_j, for $j = 1, 2, 3, 4$, can be determined (or judiciously guessed based on other known structures), the PISEMA function can be inverted to give orientation information.

The powder spectrum analysis in previous sections gives information on the degeneracies ε_2, ε_3, and ε_4. Since the values of ε_j are ±1, there are a total of $2^3 = 8$ possibilities. The only equation to restrict possibilities is Eq. [11], whose solution must be in the interval from -1 to 1. If (σ, ν) is in the elliptical section of the powder pattern (see Fig. 3), then the only two of the combinations of $(\varepsilon_2, \varepsilon_3)$ that give suitable solutions for x are those for which ε_2 and ε_3 have opposite sign; this is why there are only four solutions for (x, y, z) for (σ, ν) in this portion of the powder spectrum. Thus, Eqs. [9], [11], and [12] give a straightforward method for finding orientations (x, y, z) associated with a given PISEMA resonance when $\alpha = 0^\circ$.

For the case $\alpha \neq 0^\circ$, finding the orientation of the chemical shift principal axis frame with respect to $\vec{B}_0$ requires solving the system in Eq. [1] with $x^2 + y^2 + z^2 = 1$. As in the $\alpha = 0^\circ$ case, z can be eliminated from the equations in Eq. [1] to obtain a system

$$\begin{cases} 1 = x^2 + y^2 + z^2 \\ \sigma = (\sigma_{11}-\sigma_{33})x^2 + (\sigma_{22}-\sigma_{33})y^2 + \sigma_{33} \\ \sigma = (\sigma_{11}+\sigma_{33}\cos^2\alpha\tan^2\beta)\,x^2 + \sigma_{33}\sin(2\alpha)\tan^2\beta\,xy \\ \qquad +\, (\sigma_{22}+\sigma_{33}\sin^2\alpha\tan^2\beta)y^2 - 2\varepsilon_2\sigma_{33}\cos\alpha\,\hat{\nu}\,x \\ \qquad +\, 2\varepsilon_2\sigma_{33}\sin\alpha\,\hat{\nu}\,y + \sigma_{33}\cot^2\beta\,\hat{\nu}^2, \end{cases} \qquad [13]$$

where

$$\hat{\nu} = \tan\beta\sec\beta\sqrt{\frac{1}{3}\left(\frac{2\varepsilon_1|\nu|}{\nu_\parallel}+1\right)}.$$

Geometrically, the last two equations in Eq. [13] above describe ellipses in the xy plane. These equations can best be solved for x and y using numerical methods to find the intersection of these ellipses. In this process, two sign degeneracies are introduced so that there will be 0, 1, 2, or 4 solutions for (x, y), depending on the values of σ_{11}, σ_{22}, σ_{33}, $\nu_\parallel$, α, and β. Finally, having solved for x and y, the value of z can be found using the condition $x^2 + y^2 + z^2 = 1$, which introduces a fifth sign degeneracy. Thus, for $\alpha \neq 0$, there are 5 sign degeneracies to produce a total of 0, 8, 16, or 32 orientations for each given PISEMA resonance.

There has been no discussion of the degeneracy ε_1 so far; however, the powder spectrum does give some information on ε_1. The dipolar splitting ν lies in the interval from $-\nu_\parallel/2$ to $\nu_\parallel$. From this information alone, we know that if $|\nu| > \nu_\parallel/2$ then the sign of ν must be $+1$, but we have no information on the sign of ν if $|\nu| \leq \nu_\parallel/2$. This means that 1D spectra give little information about ε_1.

For situations in which $\alpha = 0^\circ$ or $|\sin\beta|$ is small, the 2D powder pattern gives more information on ε_1. Figure 5A shows the upper half of the doublet powder pattern divided into three disjoint regions A, B, and C. All of the resonances in region A must have $\varepsilon_1 = +1$, since region A lies on one side of the symmetry

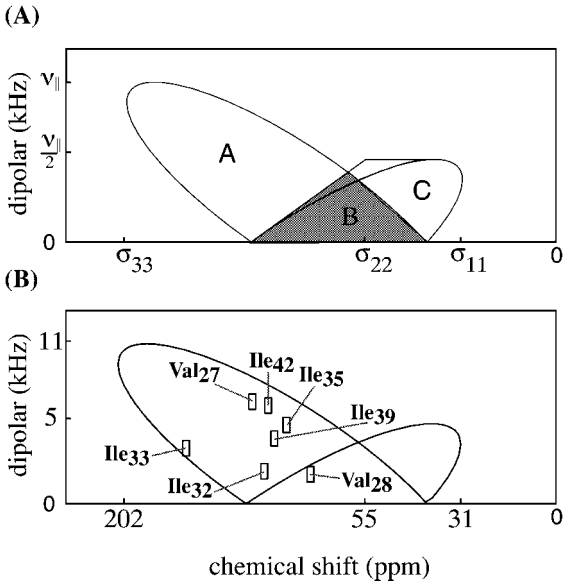

FIG. 5. (A) The powder pattern for $(\sigma, |\nu|)$ gives added insight into the degeneracy ε_1. If the resonance is in the section labeled A, then the sign of ν is $\varepsilon_1 = +1$; if the resonance is in the section labeled C, then the sign of ν is $\varepsilon_1 = -1$. But, for resonances in the section labeled B, there is no information on the sign of ν. (B) The simulated powder pattern for the M2 transmembrane peptide from influenza A is plotted with the resonances for Val^{27}, Val^{28}, Ile^{32}, Ile^{33}, Ile^{35}, Ile^{39}, and Ile^{42}. These resonances are plotted as 6 ppm by 2 kHz boxes to account for the experimental error reported in (*12*). The resonances for Val^{27}, Ile^{32}, Ile^{33}, Ile^{35}, Ile^{39}, and Ile^{42} fall in region A of the powder; hence, $\varepsilon_1 = +1$ for these residues.

line $\nu = 0$ and contains resonances whose dipolar splitting is greater than $\nu_\parallel/2$. Region C also resides completely on one side of the line $\nu = 0$. Further, the dipolar splitting of the resonances in region C will have the opposite sign of those in region A; so, $\varepsilon_1 = -1$ for resonances in region C. Finally, resonances in region B could have either $+1$ or -1 for ε_1.

In Fig. 5B, PISEMA resonances for the M2 transmembrane peptide from influenza A are plotted along with the simulated ridge plot of the powder pattern. The resonances for Val^{27}, Ile^{32}, Ile^{33}, Ile^{35}, Ile^{39}, and Ile^{42} fall into region A of the powder pattern; hence the ε_1 degeneracy for each of these resonances is resolved with $\varepsilon_1 = +1$.

With only this information about ε_1, Table 1 demonstrates the results of using Eqs. [9], [11], and [12] to compute orientations for peptide planes from PISEMA data for the M2 transmembrane peptide. Chemical shift tensor elements for individual sites are taken from (*12*), and the values in Table 1 are in agreement with calculations in (*12*).

4.3. PISA Wheels

In theory, the structure of the protein backbone can be determined, assuming standard peptide bond geometry, from the orientation of each peptide plane with respect to the magnetic field direction (*19, 20*). The structure is determined only up to certain *chiral* degeneracies due to the invariance of π with respect to the reflection sending (x, y, z) to $(x, -y, z)$.

Rather than determining all the structural parameters, often a better approach is to begin with a simpler two parameter model for each helical segment and then refine the model further. When a PISEMA experiment is performed on an α-helix, a recognizable pattern of resonances occurs. The orientation of the helix with respect to the magnetic field is then determined from this pattern. The orientation of a regular, straight α-helix is described in terms of two parameters: a tilt or *slant angle* τ and a rotation angle or *polar index* ρ_0 which will be described below. The term *Polar Index Slant Angle (PISA) wheel* describes a particular fourth order curve that fits a resonance pattern which occurs when the helix is tilted at an angle τ with respect to the magnetic

TABLE 1
Orientations Computed Using Data for M2 Transmembrane Peptide

Residue	Degeneracies				Orientation information				
—	ε_1	ε_2	ε_3	ε_4	x	y	z	$\phi(^\circ)$	$\theta(^\circ)$
Val^{27}	1	−1	1	−1	−.46	−.44	−.77	−136.6	140.2
	1	−1	1	1	−.46	.44	−.77	136.6	140.2
	1	1	−1	−1	.46	−.44	.77	−43.5	39.7
	1	1	−1	1	.46	.44	.77	43.5	39.7
Val^{25}	1	−1	1	−1	−.32	−.73	−.61	−113.7	127.6
	1	−1	1	1	−.32	.73	−.61	113.7	127.6
	1	1	−1	−1	.32	−.73	.61	−66.2	52.4
	1	1	−1	1	.32	.73	.61	66.2	52.4
	−1	−1	1	−1	−.32	−.87	−.38	−110.2	112.4
	−1	−1	1	1	−.32	.87	−.38	110.2	112.4
	−1	1	−1	−1	.32	−.87	.38	−69.8	67.6
	−1	1	−1	1	.32	.87	.38	69.8	67.6
Ile^{32}	1	−1	1	−1	−.10	−.72	−.69	−97.8	133.4
	1	−1	1	1	−.10	.72	−.69	97.8	133.4
	1	1	−1	−1	.10	−.72	.69	−82.2	46.6
	1	1	−1	1	.10	.72	.69	82.2	46.6
Ile^{33}	1	−1	1	−1	.33	−.33	−.89	−44.9	152.5
	1	−1	1	1	.33	.33	−.89	44.9	152.5
	1	1	−1	−1	−.33	−.33	.89	−135.1	27.5
	1	1	−1	1	−.33	.33	.89	135.1	27.5
Ile^{35}	1	−1	1	−1	−.58	−.46	−.67	−141.5	132.4
	1	−1	1	1	−.58	.46	−.67	141.5	132.4
	1	1	−1	−1	.58	−.46	.67	−38.5	47.6
	1	1	−1	1	.58	.46	.67	38.5	47.6
Ile^{39}	1	−1	1	−1	−.32	−.62	−.72	−117.2	135.8
	1	−1	1	1	−.32	.62	−.72	117.2	135.8
	1	1	−1	−1	.32	−.62	.72	−62.8	44.2
	1	1	−1	1	.32	.62	.72	62.8	44.2
Ile^{42}	1	−1	1	−1	−.52	−.42	−.74	−140.9	138.0
	1	−1	1	1	−.52	.42	−.74	140.9	138.0
	1	1	−1	−1	.52	−.42	.74	−39.1	42.0
	1	1	−1	1	.52	.42	.74	39.1	42.0

Note. Computation of orientations associated with PISEMA data for the M2 transmembrane peptide from influenza A. Based solely on powder pattern analysis, $\varepsilon_1 = +1$ for each given residue, except Val^{28}. To satisfy the system in Eq. [10], ε_2 and ε_3 must have opposite sign. The orientation of $\vec{B}_0$ in **PAF** is calculated using Eqs. [9], [11], and [12] and is reported as $(x, y, z) = (\cos\phi \sin\theta, \sin\phi \sin\theta, \cos\theta)$.

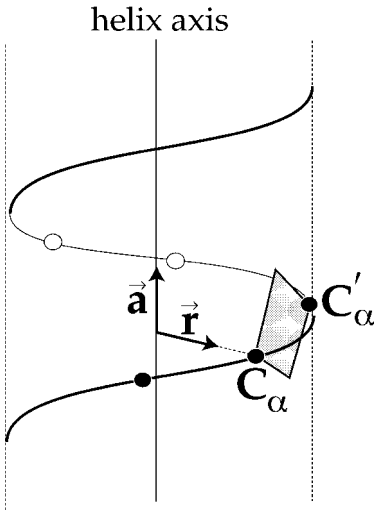

FIG. 6. The unit vectors $\vec{r}$ and $\vec{a}$ are two of the vectors in the helix axis frame, $\mathbf{HAF} = (\vec{r}, \vec{a} \times \vec{r}, \vec{a})$.

field (*2*). The tilt angle is determined by the shape and position of the wheel and the rotation angle by the pattern of assigned resonances on the wheel.

Using Eq. [*2*], the equations of the PISA wheels in the case $\alpha = 0$ can be determined. The key is to know the orientation of **PAF** with respect to a helix axis frame, **HAF**. The third vector in the helix axis frame is always the unit vector $\vec{a}$ in the direction of the helix axis, pointing in the N- to C-terminus direction. The first unit vector in this frame is the vector, $\vec{r}$, perpendicular to the helix axis and pointing from the helix axis to the *N-terminal* α-carbon in the peptide plane (see Fig. 6). Finally,

$$\mathbf{HAF} = (\vec{r},\ \vec{a} \times \vec{r}, \vec{a}),$$

and **HAF** is a right handed, orthonormal frame.

Here, the peptide planes are numbered by the residue containing the nitrogen in the plane, and so the vector $\vec{r}$ in the helix axis frame corresponding to a particular nitrogen points to the α-carbon of the *previous* residue. This scheme is important to keep in mind; otherwise, there can be some confusion about the interpretation of the rotation parameter determining the orientation of the helix. Also, other choices of the vector $\vec{r}$ are possible, such as the vector pointing from the helix axis to the nitrogen or the vector pointing from the helix axis to the midpoint of the line joining the α-carbons.

For computing PISA wheels, the key is observing there is a matrix **A** independent of the peptide plane such that

$$\mathbf{HAF} = \mathbf{PAF}\,\mathbf{A}. \qquad [14]$$

The matrix **A** depends on the particular ϕ and ψ parameters of the regular α-helix as well as on the geometry of the peptide plane. The value of **A** for $\phi = -65^\circ$ and $\psi = -40^\circ$ with standard peptide plane geometry is computed in the appendix. To find **A**, both **HAF** and **PAF** are related to a molecular frame **F** for the nitrogen in the peptide plane. The assumption is made that the principal axis $\vec{\sigma}_{33}$ always lies in the peptide plane.

The orientation of **HAF** with respect to $\vec{B}_0$ can be described by the polar coordinates ρ and τ of $\vec{B}_0$ in the helix axis frame, i.e.,

$$\vec{B}_0 = \mathbf{HAF}\,\vec{X}(\rho, \tau) \qquad [15]$$

where

$$\vec{X}(\rho, \tau) = \begin{pmatrix} \cos\rho \sin\tau \\ \sin\rho \sin\tau \\ \cos\tau \end{pmatrix}. \qquad [16]$$

By Eqs. [14] and [15],

$$\vec{B}_0 = \mathbf{PAF}\,\mathbf{A}\vec{X}(\rho, \tau)$$

so that

$$\begin{pmatrix} x \\ y \\ z \end{pmatrix} = \mathbf{A}\vec{X}(\rho, \tau) \qquad [17]$$

gives the coordinates of $\vec{B}_0$ in **PAF**, and the associated resonance is computed by substituting Eq. [17] in Eq. [2]. For fixed τ, the result gives parametric equations, parameterized by ρ, of curves called PISA wheels. PISA wheels for various τ are plotted in Fig. 7. If the helix axis $\vec{a}$ is tilted by an angle of τ from $\vec{B}_0$, then the ^{15}N PISEMA resonance for any residue lies on the PISA wheel corresponding to τ. The PISA wheels for all τ fill out the singlet powder pattern (see Fig. 7).

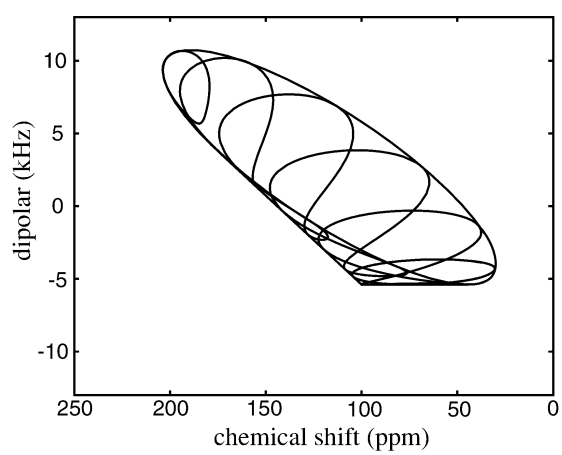

FIG. 7. The singlet powder pattern is the union of the PISA wheels for all τ. Here the simulation is created using the parameter values $\sigma_{11} = 30$ ppm, $\sigma_{22} = 100$ ppm, $\sigma_{33} = 200$ ppm, $\nu_{\|} = 10.735$ kHz, $\alpha = 0^\circ$, and $\beta = 17^\circ$.

4.4. Patterns of Resonances on PISA Wheels

In Eq. [15], the angle τ is the tilt of the helix axis with respect to $\vec{B}_0$. The angle ρ changes by 100° between subsequent peptide planes; that is, if the planes are numbered $k = 0, 1, 2, \ldots$ with the corresponding helix axis frame denoted $\mathbf{HAF}_k$ and

$$\vec{B}_0 = \mathbf{HAF}_k \vec{X}(\rho_k, \tau),$$

then

$$\rho_k = \rho_0 - k\,100^\circ. \qquad [18]$$

For fixed τ and ρ_0, substituting

$$\begin{pmatrix} x \\ y \\ z \end{pmatrix} = \mathbf{A}\vec{X}(\rho_0 - k\,100^\circ, \tau) \qquad [19]$$

in Eq. [2] for $k = 0, 1, 2, \ldots$ gives a sequence of resonances on the PISA wheel corresponding to a tilt of τ (see Fig. 8). This pattern of resonances is related to the helical wheel of the ideal helix (*2, 21*). Assigning any resonance to a value of k allows the other resonances to be assigned and ρ_0 to be determined. The values τ and ρ_0 determine the orientation of the helix with respect to $\vec{B}_0$, since they determine the coordinates of $\vec{B}_0$ in $\mathbf{HAF}_0$.

PISA wheels give a graphical approach for the interpretation of the tilt τ, but the determination of τ and ρ_0 can also be done by least squares minimization. Suppose $\pi_{o,k}$ are the observed frequencies, and

$$\pi_{c,k}(\rho_0, \tau) = \pi(\mathbf{A}\vec{X}(\rho_0 - k\,100^\circ, \tau)) \qquad [20]$$

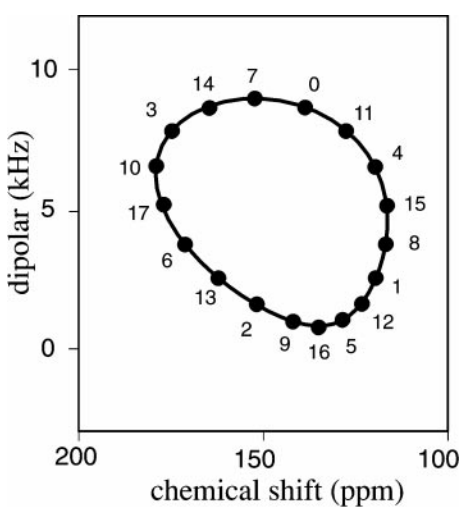

FIG. 8. A sequence of resonances on the PISA wheel for $\tau = 35^\circ$ and $\rho_0 = -10^\circ$.

are the calculated frequencies. The function

$$g(\rho_0, \tau) = \sum_k |\pi_{c,k}(\rho_0, \tau) - \pi_{o,k}|^2, \qquad [21]$$

where the sum is over all k for which data is available, can be minimized as a function of ρ_0 and τ to find the values giving the orientation of the straight α-helix most consistent with experimental observations. Note that a similar method works if only ^{15}N chemical shift data is available (*22, 23*).

Using data for the M2 transmembrane peptide from influenza **A** and using *Maple* to compute the first and second partial derivatives of g, the second derivative test from calculus shows that the absolute minimum for g occurs at $\tau = 35^\circ$ and $\rho_0 = -10^\circ$. These values are in good agreement with those reported in (*2, 22, 23*).

5. CONCLUSIONS

Solid-state NMR PISEMA experiments are powerful tools for obtaining high-resolution orientational information about membrane protein structures. Since membrane proteins have proven difficult to study using X-ray techniques and solution NMR, PISEMA and other solid-state NMR experiments occupy an important place in the list of techniques for protein structure determination. This paper adds to the methods for extracting information from PISEMA experiments.

The PISEMA function π is a map from orientations on the unit sphere to the frequency plane and gives a straightforward way of computing the ridge plots of PISEMA powder spectra. Equation [4] is an implicit equation of an ellipse that is the singlet powder pattern when $\alpha = 0^\circ$ or when $|\sin\beta|$ is small. This equation can be used to plot such powder patterns without using Hamiltonians. For other values of α and β, powder patterns can also be simulated without Hamiltonians by plotting the images of several great circles on the sphere under the PISEMA function π.

Based on the powder pattern analysis for $\alpha = 0^\circ$, four degeneracies are involved in determining peptide plane orientations associated with a particular PISEMA resonance. If these sign degeneracies can be determined or guessed, Eqs. [9], [11], and [12] demonstrate how to find orientations associated with a given PISEMA resonance.

From the PISEMA powder pattern when $\alpha = 0^\circ$ or $|\sin\beta|$ is small, the sign degeneracy, ε_1, for the dipolar splitting can be determined for some resonances, limiting the number of possible orientations associated with these resonances. Given data about adjacent residues, rough estimates of torsion angles can be computed as done by Song *et al.* (*12*). If data are available for several adjacent residues, the algorithm presented by Quine and Cross (*20*) can be used to build all possible structures for the residues. Thus, combining Eqs. [9], [11], and [12] with previously published methods gives a significant tool for determining possible structures associated with PISEMA data.

Finally, Eqs. [19] and [20] describe the patterns of resonances on a PISA wheel for an ideal membrane α-helix and are useful

in assigning resonances and in determining the tilt (τ) and rotation (ρ_0) of a membrane helix. Analytic minimization of the function in Eq. [21] gives an efficient method of determining τ and ρ_0 for a helix based on given data. Based on shapes and determination of tilt and rotation parameters, Marassi and Opella have shown that PISA wheels give an index of secondary structures (*1*). Indeed, Marassi has exhibited that the typical patterns for β-sheets in membranes also provide tilt and rotation information, and these β-sheet patterns have shapes that are quite different from the PISA wheel shapes from α-helices (*3*). These properties make PISA wheels in PISEMA spectra of oriented peptides powerful tools for qualitative assessment of secondary structures.

APPENDIX

This appendix describes the computation of the matrix **A**, used in Sections 4.3 and 4.4, giving the rotation between the helix axis frame **HAF** and the ^{15}N principal axis frame **PAF**. Both frames are related to a molecular frame **F** at the peptide plane nitrogen. The relationship of **PAF** to **F** is given by the Euler angles α and β. The relationship of **HAF** to **F** is computed from the geometry of the peptide plane and the ϕ and ψ parameters of the α-helix.

To define the nitrogen molecular frame **F**, let $\vec{f}_1$ be the unit vector in the direction of the N–C_α bond and $\vec{w}$ the unit vector in the direction of the C–N bond. Take the nitrogen molecular frame to be

$$\mathbf{F} = (\vec{f}_1,\ \vec{f}_2,\ \vec{f}_3),$$

where $\vec{f}_3 = \vec{w} \times \vec{f}_1/|\vec{w} \times \vec{f}_1|$, and $\vec{f}_2 = \vec{f}_3 \times \vec{f}_1$.

The ^{15}N chemical shift principal axis frame, **PAF**, is assumed constant in relation to **F**. Assume $\alpha = 0^\circ$ and $\beta = 17^\circ$, which are the values corresponding to a typical ^{15}N chemical shift tensor orientation for nonglycine amides (*15–17*). Further, let η be the C_α–N–H angle, and assume $\eta = 117^\circ$ based on (*25*). Then,

$$\mathbf{PAF}\begin{pmatrix}0&1&0\\0&0&1\\1&0&0\end{pmatrix} = (\vec{\sigma}_{33}, \vec{\sigma}_{11}, \vec{\sigma}_{22}) = \mathbf{F}\mathbf{R}_3(-(\beta+\eta)). \quad [A.1]$$

The computation of the helix axis frame, **HAF**, depends on the geometry of the peptide plane and the α-helix. Suppose the exterior bond angle at C_α–C–N is α, at C–N–C_α is β, and at N–C_α–C is γ. The nitrogen molecular frame $\mathbf{F}'$ in the subsequent peptide plane can be obtained from **F** by a sequence of rotations along the backbone by exterior bond angles γ, α and β, and torsion angles ϕ, ψ, and ω,

$$\mathbf{F}' = \mathbf{F}\mathbf{C},$$

where

$$\mathbf{C} = \mathbf{R}_1(\phi)\mathbf{R}_3(\gamma)\mathbf{R}_1(\psi)\mathbf{R}_3(\alpha)\mathbf{R}_1(\omega)\mathbf{R}_3(\beta)$$

and

$$\mathbf{R}_1(\theta) = \begin{pmatrix}1&0&0\\0&\cos\theta&-\sin\theta\\0&\sin\theta&\cos\theta\end{pmatrix},$$

$$\mathbf{R}_3(\theta) = \begin{pmatrix}\cos\theta&-\sin\theta&0\\\sin\theta&\cos\theta&0\\0&0&1\end{pmatrix}.$$

The rotation **C** can be written as a rotation, $\mathbf{R}(\vec{a}, \theta)$, about unit vector $\vec{a}$ by angle θ. Based on (*24*) assume

$$\alpha = 65^\circ \quad \beta = 59^\circ \quad \gamma = 70^\circ.$$

For an ideal α-helix with $\phi = -65^\circ$, $\psi = -40^\circ$, and $\omega = 180^\circ$,

$$\vec{a} \approx \begin{pmatrix}0.61\\0.76\\-0.21\end{pmatrix} \quad [A.2]$$

and $\theta = 100^\circ$. Thus,

$$\mathbf{F}' = \mathbf{R}(\mathbf{F}\vec{a}, 100^\circ)\mathbf{F}. \quad [A.3]$$

The Euclidean motion sending one peptide plane to the next also depends on a translation by a virtual bond vector from the N-terminal to the C-terminal α-carbon in a peptide plane. Again based on (*24*) assume a peptide plane geometry with C_α–C bond length 1.53Å, C–N bond length 1.34Å, and N–C_α bond length 1.45Å. Using these bond lengths and the bond angles α, β, and γ given above, the virtual bond vector from C_α to subsequent C_α can be written $\mathbf{F}\vec{v}$, where

$$\vec{v} \approx \begin{pmatrix}3.66\\-0.99\\0.00\end{pmatrix}. \quad [A.4]$$

To define the helix axis frame, **HAF**, for an ideal α-helix, it is necessary to compute the shortest vector from the initial α-carbon of the peptide plane to the axis of the helix. Placing the N-terminal α-carbon of a peptide plane at the origin, Eqs. [A.3] and [A.4] show that the Euclidean transformation

$$\vec{x} \to \mathbf{R}(\mathbf{F}\vec{a}, 100^\circ)\vec{x} + \mathbf{F}\vec{v} \quad [A.5]$$

sends one peptide plane to the subsequent plane. Repeatedly applying this transformation to the initial α-carbon will generate the α-carbon backbone of the helix. The shortest vector from the origin to the line fixed by the screw translation $\vec{x} \to \mathbf{R}(\vec{u}, \theta)\,\vec{x} + \vec{b}$ is given by Chasles' formula (*26*)

$$\frac{1}{2}\left(\cot\frac{\theta}{2}\,\vec{u} \times \vec{b} + \vec{b} - (\vec{u} \cdot \vec{b})\vec{u}\right).$$

Applying this to Eq. [A.3] shows that the shortest vector from the N-terminal α-carbon in the peptide plane to the helix axis is $\mathbf{F}\vec{p}$ where

$$\vec{p} = \frac{1}{2}(\cot 50^\circ\ \vec{a} \times \vec{v} + \vec{v} - (\vec{a} \cdot \vec{v})\vec{a}) \approx \begin{pmatrix} 1.29 \\ -1.38 \\ -1.27 \end{pmatrix}.$$

Then if $\vec{r} = -\vec{p}/|\vec{p}|$, the helix axis frame is defined to be

$$\mathbf{HAF} = \mathbf{F}(\vec{r}, \vec{a} \times \vec{r}, \vec{a}) \approx \mathbf{F} \begin{pmatrix} -.57 & .55 & .61 \\ .60 & -.22 & .76 \\ .56 & .80 & -.21 \end{pmatrix}. \quad [A.6]$$

Thus, for an ideal α-helix with $\phi = -65^\circ, \psi = -40^\circ, \alpha = 0^\circ$, and $\beta = 17^\circ$, Eqs. [A.6] and [A.1] give

$$\begin{aligned} \mathbf{A} &= \mathbf{PAF}^t\,\mathbf{HAF} \\ &= \begin{pmatrix} 0 & 1 & 0 \\ 0 & 0 & 1 \\ 1 & 0 & 0 \end{pmatrix} \mathbf{R}_3(\beta + \eta)(\vec{r}, \vec{a} \times \vec{r}, \vec{a}) \qquad [A.7] \\ &\approx \begin{pmatrix} -0.83 & 0.55 & -0.09 \\ 0.56 & 0.80 & -0.21 \\ -0.04 & -0.22 & -0.97 \end{pmatrix}. \end{aligned}$$

ACKNOWLEDGMENTS

This work was supported by the National Science Foundation, DMB 9986036 (JRQ and TAC), DMS 9972858 (JRQ), and DBI 9602233 (JKD). This work was largely performed at the National High Magnetic Field Laboratory supported by NSF Cooperative Agreement (DMR 9527035) and the State of Florida.

REFERENCES

1. F. M. Marassi and S. J. Opella, A solid-state NMR index of helical membrane protein structure and topology, *J. Magn. Reson.* **144,** 150–155 (2000).
2. J. Wang, J. K. Denny, C. Tian, S. Kim, Y. Mo, F. A. Kovacs, Z. Song, Z. Gan, R. Fu, J. R. Quine, and T. A. Cross, Imaging membrane protein helical wheels, *J. Magn. Reson.* **144,** 162–167 (2000).
3. F. M. Marassi, A simple approach to membrane protein secondary structure and topology based on NMR spectroscopy, *Biophys. J.* **80,** 994–1003 (2000).
4. C. H. Wu, A. Ramamoorthy, and S. J. Opella, High-resolution heteronuclear dipolar solid-state NMR spectroscopy, *J. Magn. Reson.* **109,** 270–282 (1994).
5. F. Tian, Z. Song, and T. A. Cross, Orientational constraints derived from hydrated powder samples by two-dimensional PISEMA, *J. Magn. Reson.* **135,** 227–31 (1998).
6. M. Linder, A. Höhener, and R. R. Ernst, Orientation of tensorial interactions determined from two-dimensional NMR powder spectra, *J. Chem. Phys.* **73,** 4959–4970 (1980).
7. M. Bak, J. T. Rasmussen, and N. C. Nielsen, SIMPSON: A general simulation program for solid-state NMR spectroscopy, *J. Magn. Reson.* **147,** 296–330 (2000).
8. C. H. Wu, A. Ramamoorthy, L. M. Gierasch, and S. J. Opella, Simultaneous characterization of the amide 1H chemical shift, 1H-15N dipolar, and 15N chemical shift interaction tensors in a peptide bond by three-dimensional solid-state NMR spectroscopy, *J. Am. Chem. Soc.* **117,** 6148–6149 (1995).
9. A. Ramamoorthy and S. J. Opella, Two-dimensional chemical shift/heteronuclear dipolar coupling spectra obtained with polarization inversion spin exchange at the magic angle and magic-angle sample spinning (PISEMAMAS), *Solid State NMR* **4,** 387–392 (1995).
10. A. Ramamoorthy, L. M. Gierasch, and S. J. Opella, Resolved two-dimensional anisotropic-chemical-shift/heteronuclear dipolar coupling powder-pattern spectra by three-dimensional solid-state NMR spectroscopy, *J. Magn. Reson.* Series B **110,** 102–106 (1996).
11. A. Ramamoorthy, C. H. Wu, and S. J. Opella, Magnitudes and orientations of the principal elements of the ^{1}H chemical shift, ^{1}H–^{15}N dipolar coupling, and ^{15}N chemical shift interaction tensors in $^{15}N_\epsilon$1-tryptophan and $^{15}N_\pi$-histidine side chains determined by three-dimensional solid-state NMR spectroscopy of polycrystalline samples, *J. Am. Chem. Soc.* **119,** 10479–10486 (1997).
12. Z. Song, F. A. Kovacs, J. Wang, J. K. Denny, S. C. Shekar, J. R. Quine, and T. A. Cross, Transmembrane domain of M2 protein from influenza A studied by solid-state ^{15}N polarization inversion spin exchange at magic angle NMR, *Biophys. J.* **79,** 7676–775 (2000).
13. W. Mai, W. Hu, C. Wang, and T. A. Cross, Orientational constraints as three-dimensional structural constraints from chemcial shift anisotropy: The polypeptide backbone of gramicidin A in a lipid bilayer, *Protein Sci.* **2,** 532–542 (1993).
14. D. K. Lee, R. J. Wittebort, and A. Ramamoorthy, Characterization of ^{15}N chemical shift and ^{1}H–^{15}N dipolar coupling interactions in a peptide bond of uniaxially oriented and polycrystalline samples by one-dimensional dipolar chemical shift solid-state NMR spectroscopy, *J. Am. Chem. Soc.* **120,** 8868–8874 (1998).
15. C. J. Hartzell, M. Whitfield, T. G. Oas, and G. P. Drobny, Determination of the ^{15}N and ^{13}C chemical shift tensors of L–[^{13}C]alanyl-L-[^{15}N]alanine from the dipole-coupled powder patterns, *J. Am. Chem. Soc.* **109,** 5966–5969 (1987).
16. T. G. Oas, C. J. Hartzell, F. W. Dahlquist, and G. P. Drobny, The amide ^{15}N chemical shift tensors of four peptides determined from ^{13}C dipole-coupled chemical shift powder patterns, *J. Am. Chem. Soc.* **109,** 5962–5966 (1987).
17. Q. Teng and T. A. Cross, The *in situ* determination of the ^{15}N chemical-shift tensor orientation in a polypeptide, *J. Magn. Reson.* **85,** 439–447 (1989).
18. S. J. Opella, F. M. Marassi, J. J. Gesell, A. P. Valente, Y. Kim, M. Oblatt-Montal, and M. Montal, Structures of the M2 channellining segments from nicotinic acetylcholine and NMDA receptors by NMR spectroscopy, *Nat. Struct. Biol.* **6,** 374–379 (1999).
19. T. A. Cross and S. J. Opella, Protein structure by solid state nuclear magnetic resonance. Residues 40 to 45 of bacteriophage fd coat protein, *J. Mol. Biol.* **182,** 367–81 (1985).
20. J. R. Quine and T. A. Cross, Protein structure in anisotropic environments: Unique structural fold from orientational constraints, *Concepts in NMR* **12,** 71–82 (2000).
21. M. Schiffer and A. B. Edmundson, Use of helical wheels to represent the structures of protein and to identify segments with helical potential, *Biophys. J.* **7,** 121–135 (1967).
22. F. A. Kovacs and T. A. Cross, Transmembrane 4-helix bundle of influenza A M2 protein channel: Structural implications from helix tilt and orientation, *Biophys. J.* **73,** 2511–2517 (1997).
23. F. A. Kovacs, J. K. Denny, Z. Song, J. R. Quine, and T. A. Cross, Helix tilt of the M2 transmembrane peptide from influenza A virus: An intrinsic property, *J. Mol. Biol.* **295,** 117–125 (2000).
24. R. A. Engh and R. Huber, Accurate bond and angle parameters for X-ray protein structure refinement, *Acta Crystallogr. Sect. A* **47,** 392–400 (1991).
25. A. Kvick, A. Al-Karaaghouli, and T. Koetzle, Deformation electron density of α-glycylglycine at 82 K. I. The neutron diffraction study, *Acta Crystallogr. Sect. B* **33,** 3796–3801 (1997).
26. D. Hestenes, "New Foundations for Classical Mechanics," Kluwer Academic, Dordrecht/Norwell, MA (1986).